Quantitative analysis of decay transients applied to a multi-mode pulsed cavity ring-down experiment.

Naus, H.; van Stokkum, I.H.M.; Hogervorst, W.; Ubachs, W.M.G.

published in
Applied Optics
2001

DOI (link to publisher)
10.1364/AO.40.004416

document version
Publisher's PDF, also known as Version of record

Quantitative analysis of decay transients applied to a multimode pulsed cavity ringdown experiment

Hans Naus, Ivo H. M. van Stokkum, Wim Hogervorst, and Wim Ubachs

The intensity and noise properties of decay transients obtained in a generic pulsed cavity ringdown experiment are analyzed experimentally and theoretically. A weighted nonlinear least-squares analysis of digitized decay transients is shown that avoids baseline offset effects that induce systematic deviations in the estimation of decay rates. As follows from simulations not only is it a method that provides correct estimates for the values of the fit parameters, but moreover it also yields a correct estimate of the precision of the fit parameters. It is shown experimentally that a properly aligned stable optical resonator can effectively yield monoexponential decays under multimode excitation. An on-line method has been developed, based on a statistical analysis of the noise properties of the decay transients, to align a stable resonator toward this monoexponential decay. © 2001 Optical Society of America

OCIS codes: 000.4430, 120.2230, 300.0300.

1. Introduction

Since the invention of a technique known as cavity ringdown spectroscopy[1] (CRDS) a large number of applications have been described. Also a number of variants of this versatile and sensitive laser technique for measuring absorption resonances have been proposed. They all exhibit the major advantages of CRDS: long effective absorption path lengths combined with the independence of shot-to-shot fluctuations in the laser output. Although the suggestion of using Fabry–Perot cavities to enhance absorption sensitivity dates back to Kastler[2] and methods for intracavity laser absorption were demonstrated in the early days of the tunable laser,[3] cavity-enhanced techniques were initially used only for measuring mirror reflectivities.[4] The mere realization by O'Keefe and Deacon[1] that a conceptually simple setup, where two mirrors formed a stable resonator and a commonly available pulsed laser, could detect molecular absorption features with extreme sensitivity initiated a new branch of research. Applications of CRDS in molecular spectroscopy have been recently reviewed.[5,6]

Details of cavity-enhanced spectroscopic techniques and the problems associated with the measurement and interpretation of decay transients obtained from a stable resonator have been elaborated. Here a few studies are cited that gave insight into the physics of the optical decay transients and their analysis. Lehmann and Romanini[7] analyzed in detail the effects of mode structure on the optical transients obtained from a cavity. In Ref. 8 van Zee *et al*. studied the experimental conditions in which a single cavity mode is excited when short cavities and transverse-mode suppression are used; their rather complex setup requires control of the cavity length. From a statistical analysis of the observed transients the relative standard deviation in the ringdown time could be extracted. Martin *et al*.[9] discussed the implications of using single-mode Fourier-transform-limited pulses in analyzing the interference effects in the resonator producing mode-beating oscillations in the exiting waveform. Lee *et al*.[10] performed a time-domain study on cavity ringdown (CRD) signals from a resonator under pulsed laser excitations, focusing on the idealized case of a Fourier-transform-limited Gaussian laser pulse with complete mode match to the lowest cavity mode, including the subtle effects of carrier frequency detuning from this cavity mode.

The problems associated with the nonzero bandwidth of the laser source, in particular in the regime where it is nonnegligible with respect to the width of the molecular absorption features, have been dis-

When this research was performed, all the authors were with the Laser Centre, Department of Physics and Astronomy, Vrije Universiteit, De Boelelaan 1081, 1081 HV Amsterdam, The Netherlands. H. Naus is now with JDS Uniphase, Prof. Holstlaan 4, 5656 AA Eindhoven, The Netherlands. The e-mail address for W. Ubachs is wimu@nat.vu.nl.

Received 5 January 2001; revised manuscript received 2 April 2001.

0003-6935/01/244416-11$15.00/0

cussed by Jongma *et al.*,[11] Zalicki and Zare,[12] and Hodges *et al.*[13] These problems are similar to the slit-function problem encountered in classical linear absorption spectroscopy. However, correction for these effects in CRDS is nontrivial, inasmuch as each frequency component within the laser bandwidth profile gives rise to a different decay time, thus producing multiexponential decay.

In recent years several cavity-enhanced techniques have been developed exhibiting elegant features and employing continuous-wave lasers.[14–16] Ye *et al.*[17] obtained extreme absorption sensitivity of 10^{-14} cm^{-1} by combining these cavity-enhanced techniques with frequency modulation spectroscopic techniques. But the simple version of CRD with multimode excitation of a cavity by a standard laser, with typical features of 0.1-cm^{-1} bandwidth and a pulse duration of 5 ns, remains a powerful technique and has been implemented in a growing number of laboratories. If the length of the resonator is chosen to be ≈80% of the radial curvature of the mirror substrates and transverse-mode suppression is deliberately omitted, the cavity can be considered essentially white, as shown experimentally by Meijer *et al.*[18]: The transmission through the cavity is independent of wavelength.

Here we analyze and describe the noise properties of decay transients in a generic pulsed CRD experiment. We show that the transmission of a typical CRD cavity in terms of the photon number and its variance can be understood quantitatively. It is demonstrated that a nonlinear least-squares analysis of the decay transient can avoid baseline offset effects that can be responsible for systematic deviations in decay rates. A parameter α_p can be defined that characterizes the noise that originates from a Poisson-distributed counting process on a decay transient. This parameter can be employed to implement an on-line alignment procedure for the resonator; it is experimentally demonstrated that the alignment of a CRD cavity can be optimized toward a setting of monoexponential decay, even when a large number of cavity modes are excited by the incident laser pulse. In this condition effects that are due to the mode structure of the resonator can be ignored; this is the condition of a white CRD cavity.

2. Estimating the Rate of Monoexponential Decay: Analog Method

Excitation of multiple modes in an optical resonator will in principle result in a multiexponential decay of the exiting flux of photons. The multiexponentiality is caused by increasing diffraction losses for higher-order transversal TEM_{mn} modes in the resonator.[19] Because pulsed dye lasers will in general excite multiple modes of an optical resonator, the decay is in principle not monoexponential. The multiexponential character of the decay in the case of a multiple-modes-excited resonator can deviate so minimally from a single exponent that it is not discernible by any means in the recorded experimental decay. Alternatively the cavity alignment can be arranged so that the losses are equal for each excited transversal mode. Experimental decays are considered to be monoexponential if the results of a monoexponential fit greater than ≈10τ (τ is the decay time) do not indicate nonexponential or multiexponential behavior.

The purely monoexponential character of the decay is important for reliable retrieval of the absorption properties of a species contained inside the resonator. Only in this condition can the absorption coefficient $\alpha_{(\nu)}$ be estimated from the decay rate β (=1/τ) by

$$\alpha_{(\nu)} = \frac{\beta}{c} - \frac{|\ln R|}{l}, \tag{1}$$

where l is the cavity length, c is the speed of light, and R is the mirror reflectivity. Equation (1) makes the CRD technique a suitable tool for measuring direct absorption.

The principles of the methods for estimating the decay rate of an experimental transient are best explained by considering a perfect monoexponential decay in its most general form:

$$I_{(t)} = I_{\text{off}} + I_0 \exp(-\beta t), \tag{2}$$

where I_{off} accounts for an offset that could be introduced by the detection system and I_0 is the initial intensity. The decay rate can be determined in an analog way with the aid of two boxcar devices by electronic integration of part of the decay inside two successive time windows of equal width $t_g^{(1,2)}$ and a time delay $\Delta_g[\Delta_g \geq t_g^{(1)}]$ between them,[20] as depicted in Fig. 1. With

$$A = \int_{t_g^{(1)}} I_{(t)} \mathrm{d}t, \qquad B = \int_{t_g^{(2)}} I_{(t)} \mathrm{d}t, \tag{3}$$

the decay rate β follows from

$$\beta = \frac{1}{\Delta_g} \ln\left(\frac{A}{B}\right). \tag{4}$$

Some two-channel boxcars can execute Eq. (4) internally at high repetition rates with the advantage that the output signal is directly correlated to β. This detection scheme, however, requires that $I_{\text{off}} = 0$; otherwise Eq. (4) is not valid. The signal can be biased to eliminate I_{off}, or a third boxcar can be used to determine the offset of the actual ringdown signal; with $C = \int_{t_g^{(3)}} I_{(t)} \mathrm{d}t$ [width, $t_g^{(3)} = t_g^{(1,2)}$],

$$\beta = \frac{1}{\Delta_g} \ln\left(\frac{A - C}{B - C}\right). \tag{5}$$

The output signals of the boxcars must then be recorded and processed for β to be determined inasmuch as commercially available boxcar devices cannot perform the operation [Eq. (5)] directly.

In this analog method timing is important; the gate widths t_g should be equal and the time separation Δ_g between the gates accurately known and stable. The gate settings are fixed and often optimized for

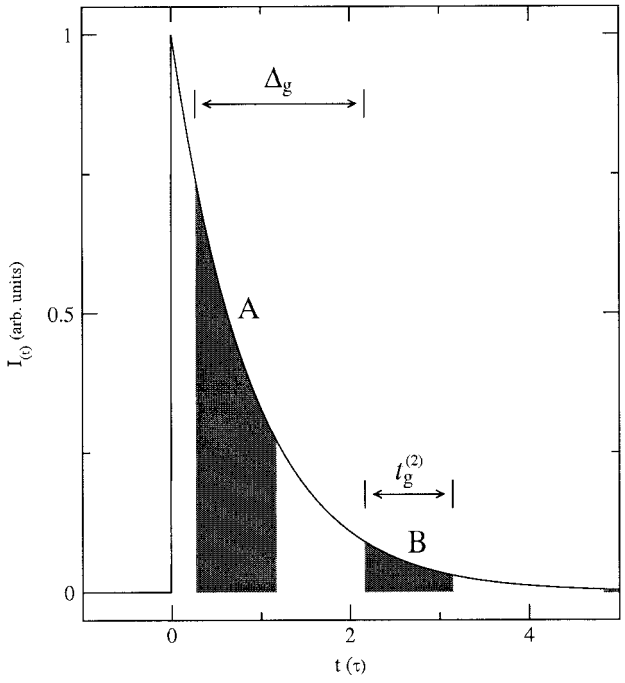

Fig. 1. Exponential decay rate estimated by integrating the decay inside two successive time windows. The situation represents settings used by Romanini and Lehmann[20] (see text). A possible third time window to estimate the baseline (see text) is not shown.

the decay signal of an empty cavity.[20] When the laser frequency is scanned over an absorption line the decay rate will increase and the (fixed) settings might no longer be optimal. Variation in the timing settings can introduce additional noise in the measured spectrum.[20] Another point of concern is that a zero offset or a known offset is necessary for this method to be able to correct for it; this baseline problem will be addressed in some detail in Section 3.

An alternative scheme for determining the decay rate introduced by O'Keefe[21] and O'Keefe *et al.*[22] uses integration of the total decay,

$$\int_0^\infty I_0 \exp(-\beta t)\mathrm{d}t = \frac{I_0}{\beta}. \tag{6}$$

The intensity independence of the signal, one of the main advantages of the CRD technique, is lost, however. Normalization with respect to the initial intensity I_0, probed separately by setting a narrow second time window, is in effect similar to the use of Eq. (5). Another analog detection scheme has been introduced[16] in which the output of the detector is logarithmically amplified to convert the exponential decay to a linearly decaying signal. The output of the logarithmic amplifier is then differentiated by an analog differentiating circuit, generating a potential that is proportional to the decay rate β. This scheme is particularly suitable when continuous-wave lasers or high-repetition-rate pulsed lasers are employed. Note that in these last two schemes $I_{\mathrm{off}} = 0$ is required.

3. Nonlinear Fit of Experimental Monoexponential Decays after Digitization

As an alternative to methods in which the signal is processed by analog electronics, the entire decay transient can be recorded, digitized, and transferred to a computer for analysis, which returns the decay rate β. Often a linear fit is used to determine the decay rate because it is easy to implement and fast. After subtraction of the baseline the logarithm of the decay is fitted to a straight line.[8,18] In Subsection 3.A we illustrate how the baseline offset could cause an incorrect estimate of decay rate β and hence of absorption coefficient $\alpha_{(\nu)}$. Subsequently unweighted and weighted fitting procedures for digitized decay transients will be analyzed and supported by simulation studies.

A. Errors Caused by Incorrect Baseline Estimation

The requirement of a zero offset, required for linearization of the transients to a logarithm scale, but also for the analog methods discussed above, can seem trivial inasmuch as the offset can be estimated from the baseline before the ringdown signal. This offset, however, must be determined accurately because a small deviation from a zero offset results in a substantial error in the estimated decay rate. Consider an exponential decay with a small offset of only 0.5% of the initial intensity I_0 and $\beta = 1$:

$$I_{(t)} = [0.005 + \exp(-t)]I_0. \tag{7}$$

The effect of the offset in an analog detection scheme with boxcars is illustrated with settings as used by Romanini and Lehmann[20]: $t_g^{(1,2)} \approx 0.5\tau_0$, $\Delta_g \approx 2\tau_0$, and the first-time window delayed by $0.25\tau_0$ with respect to t_0 (Fig. 1). Substitution of these settings in Eqs. (3) and (4) results in $\beta = 0.9748$, a deviation of 2.5%. The effect of the small offset on the logarithm of $I_{(t)}$ is clearly visible in Fig. 2. A linear (unweighted) fit over $3\tau_0$, a commonly used fit range, from t_0 to $t = 3\tau_0$ returns a decay rate of 0.9745, similar to the value estimated with the boxcar method. It can easily be verified that deviations in the decay rates depend on the fit range.

If the offset deviations for consecutive laser pulses are randomly distributed around zero, e.g., as a result of the standard deviation in the baseline estimation, errors in the estimation of the decay rate as a consequence of an offset will result in additional noise. In the case of a typical CRD wavelength scan noise in the frequency spectrum $\beta(\nu)$ will result. Averaging ringdown events can reduce this noise because the offset uncertainty will average out. The averaging procedure, however, is allowed only if individual decay transients decay with equal rates. Systematic offsets will result in a systematic error in the decay rate. A source of systematic nonzero offsets is the possible baseline shift owing to small charge effects in the detection circuit. The baseline of the output of a photomultiplier tube (PMT), for example, can shift when a signal is present.[23] Then an offset estimated before or after the ringdown event is not correct.

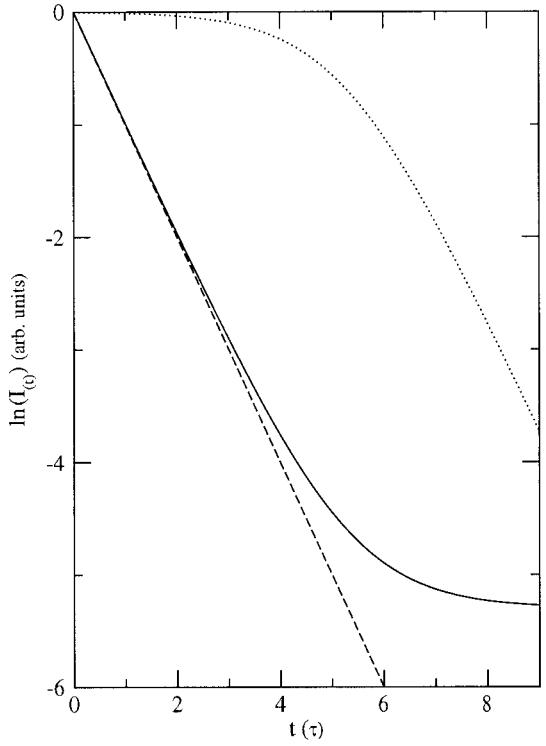

Fig. 2. Effect of small offset on the logarithm of $I_{(t)}$: solid curve, effect on the logarithm of a 0.5% biased exponential decay (see text); dashed curve, logarithm of an exponential decay with no offset; dashed curve, difference between the two logarithms.

B. Experimental Recording of Decay Transients

An experimental single-shot decay transient recorded with a typical CRDS setup is shown in Fig. 3. A Nd:YAG-pumped pulsed dye laser emitting pulses of 5-ns duration with a bandwidth of 0.05 cm^{-1} at 630 nm was used in combination with an empty cavity built from two mirrors ($R \approx 99.98\%$; Newport Super-Mirrors) with a radius of curvature of 1 m, separated by 86.5 cm. The cavity length corresponds to a cavity round-trip time of 5.7 ns. Before detection the exiting light passes through an optical bandpass filter with transmission $T_{630} = 0.856$ and a lens placed in front of the photocathode of a PMT (Thorn EMI 9658 RA, socket 9658-81-81) with an effective diameter of 42 mm, ensuring that all the light is detected. According to specifications the quantum efficiency (QE) of the PMT at 630 nm is 0.12, whereas the gain at 950 V is $\approx 0.3 \times 10^6$. Samples of the decay transient were taken every 50 ns with an 8-bit LeCroy 9450 digital oscilloscope with a bandwidth of 350 MHz.

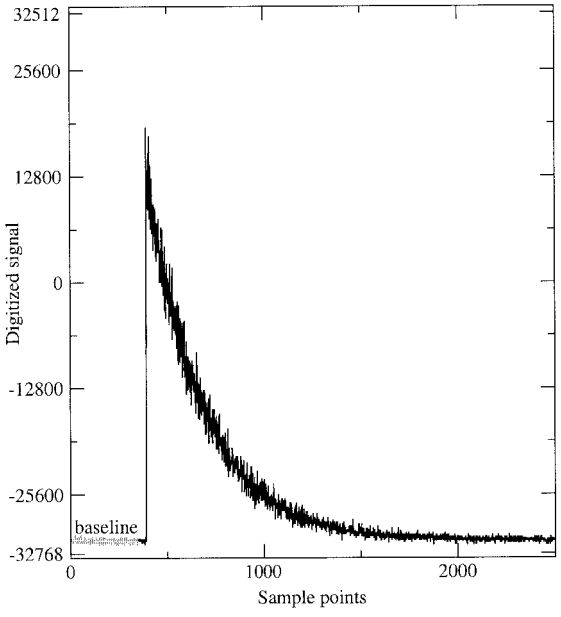

Fig. 3. Experimental single-shot decay transient as recorded with the digital oscilloscope. The signal before the ringdown event (baseline) is used to determine the offset.

The scales in Fig. 3 are in dimensionless digital coordinates to make the analysis generally applicable. For convenience the negative PMT signal is inverted. The 0–255 dynamic range of an 8-bit digitizer is represented by 7 bits + sign bit (−128–127) and through the buffer memory of the oscilloscope converted to a 16-bit representation with a minimum step size of 256.

C. Unweighted Nonlinear Fit of Experimental Decays

Although the nonlinear fit does not require a zero baseline before the decay, the original decay is first shifted vertically to a zero baseline for easier interpretation of the fitted offset. For this purpose the mean value of the signal before the ringdown event is determined over the first 350 points and is subtracted from the signal. The actual decay starts at $t = t_0 = 393$ (t in channels), but for clarity the decay is shifted along the time axis to $t_0 = 0$. The thus transposed decay, with a zero baseline and $t_0 = 0$, is used as input for the nonlinear fit. To prevent errors from a possible shift in t_0, as a result of the discreteness of the time scale, the fit does not start at t_0 but typically at $t_{st} = t_0 + 0.01\tau_0$. The maximum dynamic range of the digitizer is not fully used (in the example ≈70% is chosen) in view of the shot-to-shot intensity fluctuations. A margin to prevent clipping the signal is necessary.

To fit the decay a Levenberg–Marquardt algorithm is used. For a detailed explanation of this algorithm, see Press *et al.*[24] The results of the procedure are summarized in Table 1 (first row). The residuals of the unweighted fit (Fig. 4) show a variance that decreases over the decay transient. To test whether a power-law relation is present between the variance and the intensity of the fitted model function, the absolute value of the residuals is plotted against the expected value of the intensity of the model function on a double logarithmic scale, as shown in Fig. 5. The data in the scatterplot are fitted to a straight line with a slope of 0.453 (solid line in Fig. 5). This is close to a slope of 0.5 expected for a Poisson-distributed counting process, where the variance is proportional to the expected value. (The residuals are proportional to the square root of the number of counts.)

The deviation of the slope from the expected value

Table 1. Results of the Unweighted and Weighted Fit of the Decay Shown in Fig. 3

Fit	I_{off}	I_0^{fit}	$\beta \times 10^6$	Root-Mean-Square Error of Residuals
Unweighted	−25 (25)	44222 (102)	3452 (10)	849
Weighted	−29 (10)	44157 (212)	3444 (16)	0.96

Note: The values in parentheses represent the standard deviation.

of 0.5 can be explained by the distribution of the points in the scatterplot. At lower intensities the electronic noise, with a constant variance, is no longer negligible and the intensity dependence of the variance decreases, resulting in a lower estimate of the slope. The two dashed lines in Fig. 5 represent the functions $y = (3x)^{1/2}$ (upper line) and $y = (0.03x)^{1/2}$ (lower line). It is clearly visible that the envelope of the absolute values of the residuals is well represented by a $x^{1/2}$ dependence.

D. Statistics of a Poisson-Distributed Counting Process

The signal that is measured in a CRD experiment is proportional to the number of photons. If no gain or averaging processes are present, the variance $\mathrm{var}(I_c)$ of a Poisson-distributed counting process is equal to the expected value $E[I_c]$:

$$E[I_c] = \mathrm{var}(I_c). \tag{8}$$

When gain g is present in the detection system, the measured intensity $I_m{}^g = g(I_c)$; hence Eq. (8) is no longer valid. The relationship between the variance $\mathrm{var}(I_m{}^g)$ and the expected value $E[I_m{}^g]$ of the measurement can easily be derived, giving[25]

$$\frac{\mathrm{var}(I_m{}^g)}{E[I_m{}^g]} = g. \tag{9}$$

An average over N counting events per data point n will also change the relationship between the variance and the expected value. In a CRD experiment this can be accomplished by averaging the decay signals of N laser pulses. The expected value $E[\bar{I}_m]$ will remain the same but the variance will decrease[25]:

$$\mathrm{var}(\bar{I}_m) = \frac{1}{N^2}\sum_N \mathrm{var}(E[I_c^{(n)}]) = \frac{1}{N}\mathrm{var}(I_c). \tag{10}$$

Hence

$$\frac{\mathrm{var}(\bar{I}_m)}{E[\bar{I}_m]} = \frac{1}{N}. \tag{11}$$

In typical experimental conditions a combination of gain and averaging results in

$$\frac{\mathrm{var}(\bar{I}_m{}^g)}{E[\bar{I}_m{}^g]} = \frac{g}{N} = \alpha_p^{(N)}, \tag{12}$$

defining a parameter α_p, which describes the relationship between the variance and the expected value of a measurement of a Poisson-distributed counting process. It can be usefully applied, as shown below.

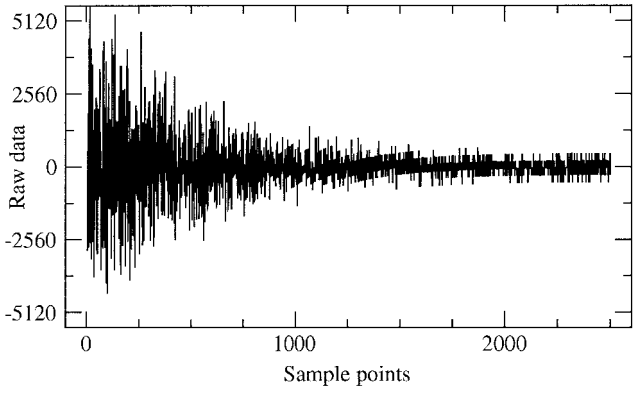

Fig. 4. Residuals of a monoexponential fit to the decay shown in Fig. 3. Discretization effects due to the 8-bit resolution of the digitizer are visible on the right-hand side. In the first part of the decay the noise due to Poisson statistics is dominant.

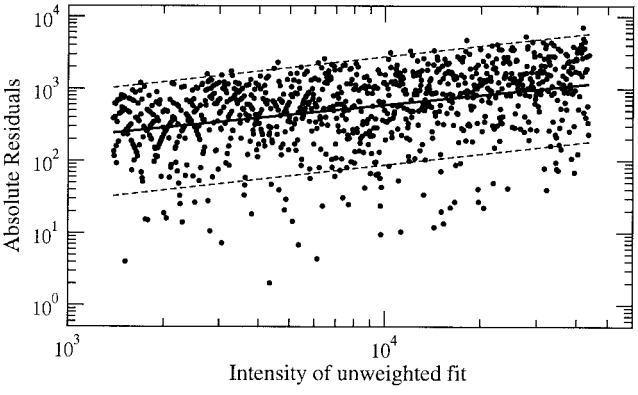

Fig. 5. Scatterplot of the absolute values of the residuals from the unweighted fit versus the fitted intensity. The slope (0.453) of a line fitted to the data (solid line) in the scatterplot indicates that the intensity-dependent noise on the recorded transient originates from a Poisson-distributed counting process.

E. Weighted Nonlinear Fit of Experimental Decays

From the residuals of the exponential fit shown in Fig. 4 it is clear that the noise during the decay is not constant. If the standard deviations in a measurement vary by a factor of 3 or more, it is necessary to take the probabilistic properties into account in the fitting.[26,27] Only by such a procedure can the residuals and the results of the fit be evaluated reliably. In a weighted least-squares fit[24] the expected variance in a data point is used to weight that point; to perform a correctly weighted fit it is necessary to know the expected variance. A perfectly weighted fit will return weighted residuals that behave randomly around zero with a constant variance of one.

From Figs. 4 and 5 it follows that the noise in the decay, the variance, originates from two sources: (discretized) electronic noise and intensity-dependent Poisson noise. Assuming that the two noise sources are independent, the total expected variance var^t is equal to

$$\mathrm{var}_{(I)}{}^t = \mathrm{var}^e + \mathrm{var}_{(I)}{}^p, \tag{13}$$

where var^e is the expected (constant) variance due to electronic noise and $\mathrm{var}_{(I)}{}^{\mathrm{p}}$ is the intensity-dependent variance that is due to the Poisson-distributed counting process. The expected electronic variance can easily be determined from the standard deviation of the mean value of the baseline before the ringdown event, which has already been used to shift the original transient; $\mathrm{var}^e = \sigma_{\mathrm{base}}{}^2$. The Poisson variance var^p, however, is not known beforehand because it is intensity dependent. Nevertheless it is possible to estimate the expected variance over the total decay and to perform a weighted fit.

Equation (12) gives the relationship between the expected value of the intensity and the variance for a general Poisson-distributed counting process with a system gain g and an average over N counting events per data point. When the expected value $E[I_m]$ for the intensity is time dependent, the variance $\mathrm{var}(I_m)$ is also time dependent, but their ratio α_p remains constant over the total decay. This relationship in combination with an unweighted fit enables the estimation of the expected Poisson variance var^p. From the results of the unweighted nonlinear fit (Table 1) the expected intensity $E[I_{(k)}]$ can be calculated for each point k on the decay transient. The value of α_p can now be estimated with

$$\begin{aligned}\hat{\alpha}_p &= \frac{1}{K}\sum_{k=1}^{K}\frac{\mathrm{var}[I_m^{(k)}]}{E[I_{(k)}]} \\ &= \frac{1}{K}\sum_{k=1}^{K}\frac{\{I_m^{(k)} - E[I_{(k)}]\}^2}{E[I_{(k)}]},\end{aligned} \tag{14}$$

where the circumflex indicates the estimator of α. Equation (14) gives the true value for α_p when no other noise is present, but the additional electronic noise calls for a simple correction term. The term $\mathrm{var}[I_m{}^{(k)}]$ in Eq. (14) represents the total variance, which is the sum of the electronic variance and the Poisson variance. Because the electronic variance var^e is known from the baseline before the ringdown event, it can be subtracted from $\mathrm{var}[I_m{}^{(k)}]$ and a reliable value of α_p can be estimated:

$$\begin{aligned}\hat{\alpha}_p &= \frac{1}{K}\sum_{k=1}^{K}\frac{\mathrm{var}[I_m^{(k)}] - \mathrm{var}^e}{E[I_{(k)}]} \\ &= \frac{1}{K}\sum_{k=1}^{K}\frac{\{I_m^{(k)} - E[I_{(k)}]\}^2 - \sigma_{\mathrm{base}}{}^2}{E[I_{(k)}]}.\end{aligned} \tag{15}$$

Combining Eqs. (12), (13), and (15), we find the expected $\mathrm{var}_{(I)}{}^t$ that is needed for the weighted fit.

This procedure is valid for estimating the total expected variance $\mathrm{var}_{(I)}{}^t$ because the Poisson noise at the low intensities of the signal is negligible with respect to electronic noise. It is thus not necessary to take into account the Poisson probability density function of the counting process for small count values. Note that the estimation of the weight factors relies on the results of the unweighted fit. An incorrect unweighted fit will result in an incorrect estimate of α_p and subsequently incorrect weight factors. It is therefore important to check the results of the unweighted fit and the values determined for α_p before proceeding to the weighted fit. Large differences between the estimated parameters of the unweighted and weighted fit can indicate unreliable weight factors or nonexponential decay or both. An indication of an incorrect estimate of the weight factor is the value of α_p. It is in principle equal for each decay if the data-acquisition settings are kept constant. Strong deviations from the average value of α_p indicate unreliable fit results.

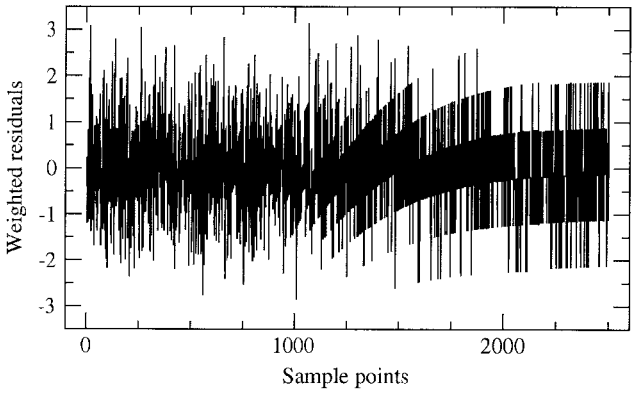

Fig. 6. Residuals of a weighted monoexponential fit to the decay as shown in Fig. 3.

The Levenberg–Marquardt algorithm used for the weighted least-squares fit is similar to the unweighted-fit algorithm.[24] The weighted residuals resulting from the weighted fit, shown in Fig. 6, with weights determined by the procedure presented here are satisfactory inasmuch as they show a constant variance with a standard deviation of 0.96. Results of the weighted fit are summarized in the second row of Table 1. Comparison of the estimated parameters from the weighted and unweighted fit reveals only small differences, and the standard deviations of the parameters estimated with the unweighted fit are of the same order of magnitude as those obtained from the weighted fit.

Note that the weighted fit returns a smaller uncertainty for the offset than in the case of the unweighted fit. The standard deviations of the unweighted fit (Table 1) are in principle a lower bound because the rms error of the residuals is much larger than one. This paradox can be explained by the intensity dependence of the weight factor. The information on the initial intensity $I_0{}^{\mathrm{fit}}$ and the decay rate β is mainly present in the first part of the decay where the accuracy of the collected data points is lowest owing to Poisson noise. In the tail of the

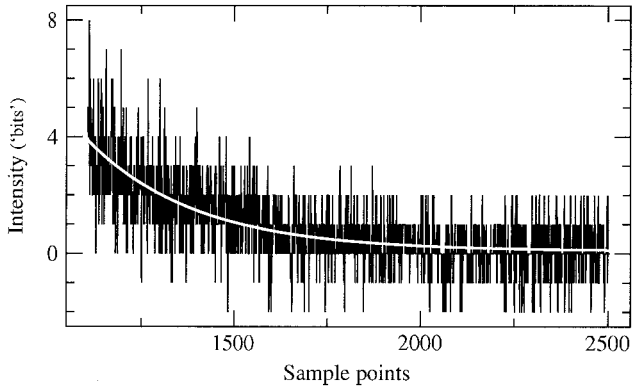

Fig. 7. Effect of the 8-bit resolution of the digitizer. The digitized signal will remain constant during a certain time interval (neglecting noise) until the slowly decreasing signal reaches the next bit level. This effect results in striation in the residuals (Fig. 6) of the fit. Solid white curve, fitted decay.

decay, where information on the offset is present, only electronic noise is present. The unweighted fit assumes a constant noise level, resulting in nonreliable estimates of the uncertainties; the uncertainties for I_0 and β are estimated too low, whereas the uncertainty for the I_{off} is estimated too high. In this example the fitted offset I_{off} is 0.07% of I_0^{fit}, but if this offset is not accounted for (I_{off} is kept fixed at zero), the decay rate estimate is 0.3% higher (3455 versus 3444). This deviation cannot be neglected because the estimated uncertainty in the decay rate is smaller than 0.5%, i.e., even a small offset cannot be ignored.

The residuals of the weighted fit show a discrete distribution on the right-hand part that can be explained by the intensity dependence of the weight factor. At high intensities of the decay transient the weight factor is not constant and will decrease with intensity because the Poisson contribution is dominant, and, as a consequence, the discrete steps due to the bit resolution will wash out in the weighted residuals. The weight factor becomes constant at low intensities because the contribution of the Poisson noise is negligible compared with the constant electronic noise; the discrete steps remain.

A second remarkable feature is the striation in the residuals, which is an effect of the limited resolution of the 8-bit digitizer. After several decay times τ ($1/\beta$) the intensity change in time is too small to be detected by the digitizer. The digitized signal will remain constant during a certain time interval (neglecting noise) until the signal reaches the next bit level, as shown in Fig. 7. The calculated intensity following the fit is not discretized, and the residual ($I_{\mathrm{meas}} - I_{\mathrm{calc}}$) will show a curved behavior after $\approx 4\tau$.

F. Simulation Study of the Nonlinear Fitting Method

CRDS decay transients from experiments are probabilistic in nature because of the underlying photon-counting process. In fact, in the fitting it is necessary to take into account the probabilistic properties consistently. Only by such a procedure can the residuals of the fit be evaluated and the model adequately established.[26,28] It is the purpose of this simulation study to demonstrate quantitatively the advantages of the weighted nonlinear fit with a typical CRDS decay.

For the simulation study a decay of 2048 channels was chosen, with a lifetime τ (reciprocal of the decay rate β) of 250 channels ($\beta = 4 \times 10^{-3}$ channel^{-1}). Poisson-distributed counts with an exponentially decaying mean were simulated. The amplitude of the decay in the first channel I_0 was 400, the baseline I_{off} was 1, and the standard deviation of the electronic noise was 2. These values were chosen to mimic a CRDS decay as shown in Fig. 3. Two ways of estimating the unknown parameters are compared: (a) unweighted nonlinear least squares and (b) weighted nonlinear least squares with weights derived from the variance defined in Eq. (13). According to Carroll and Ruppert[27] this weighted least-squares estimate is equal to the maximum likelihood estimate, which is the best possible. For the actual weighted fit we proceed iteratively: First, for the weighting function we use the profile estimated from an unweighted fit; second, we use the resulting profile to perform a refined weighted fit (so-called iteratively reweighted least squares[27]). This refinement is a safeguard; it turned out not to improve the fit results.

From a single simulation we can already observe that the weighted residuals of a weighted fit are satisfactory, i.e., they behave randomly and show a constant variance (comparable with Fig. 6), whereas the residuals of an unweighted fit behave as in Fig. 4. However, to investigate quantitatively the properties of a weighted versus an unweighted fit 1024 simulations were performed. This resulted in 1024 realizations of the estimates ($\hat{\beta}$, $\hat{I}_0$, and $\hat{I}_{\mathrm{off}}$) and their standard errors ($\hat{\sigma}_\beta$, $\hat{\sigma}_{I_0}$, and $\hat{\sigma}_{\mathrm{off}}$; for calculation of these standard errors, see, e.g., Ref. 26). We summarize the resulting estimates for the parameters and their standard errors by estimating smoothed probability densities using the S-plus function, ksmooth.[29] Figure 8(a) depicts the distribution of deviations in the decay rate parameter $\Delta_\beta = \hat{\beta} - \beta$ (the difference between the estimated and the real value) of a weighted nonlinear least-squares fit. It is symmetric around zero with a rms value of 17×10^{-6} channel^{-1}. The distribution of the standard error $\hat{\sigma}_\beta$ [Fig. 8(b)] narrowly peaks around 17×10^{-6}. The ratio of the deviation and the estimated standard error should be distributed approximately as a Student's t-variable with the degrees of freedom df equal to the number of data points N minus the number of parameters [Eqs. (3)]. (In this case, $df = 2045$, the t_{df} distribution is practically identical to the normal distribution.) The distribution of this ratio is depicted by the solid curve in Fig. 8(c), whereas the dotted curve represents the t_{df} distribution. There is a great similarity. The small differences that are present are attributed to the linear approximation of the standard errors[26] and to the inadequacy of the assumed normal distribution to describe small numbers of Poisson-distributed counts.

A comparison with the results of an unweighted fit

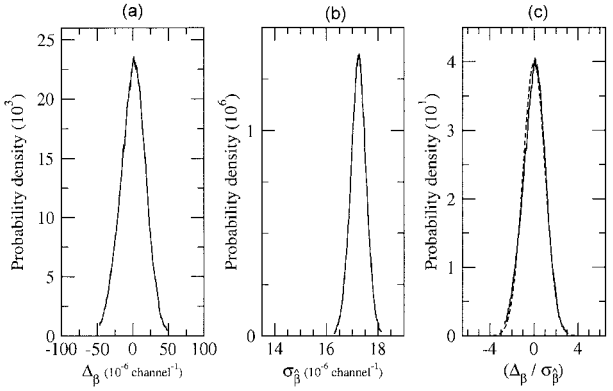

Fig. 8. Distributions estimated from the weighted fit: (a) deviation Δ_β of the estimated decay rate parameter β; (b) approximate standard error σ_β; (c) solid curve, ratio of Δ_β and σ_β; dashed curve, t_{df} distribution.

can be made for which the residuals do not behave well (Fig. 4). The summary of decay parameters for this case is shown in Fig. 9. Note that the distribution of the deviation in Fig. 9(a) is wider by a factor of ~1.5 compared with that in Fig. 8(a). The estimated standard errors are on average smaller [compare Figs. 8(b) and 9(b)]. Most important, the differences between the solid and the dashed curves are much more pronounced in Fig. 9(c) than in Fig. 8(c); note the tails in Fig. 9(c). This means that for large deviations the unweighted fit predicts more precise results than actually achieved.

The results in Table 2 confirm that the weighted fit is superior to the unweighted fit. The rms deviation Δ_β of the unweighted fit is larger than that of the weighted fit. Only with the weighted fit is the rms standard error $\hat\sigma_\beta$ equal to the rms deviation Δ_β,

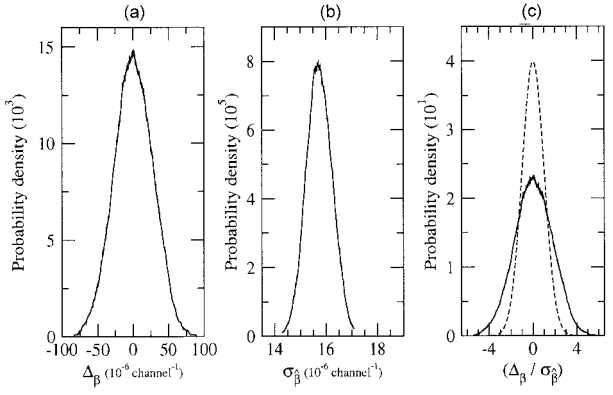

Fig. 9. Distributions estimated from an unweighted fit. Layout as in Fig. 8.

which is necessary for a consistent fit. This consistency is also present in the amplitude and baseline parameters. The weighted rms error was 1.0 (rms average). Comparing Table 2 with the fit of the experimental data (Table 1), we note agreement with the standard error of the decay rate parameter $\hat\sigma_\beta$. Taking into account the ratio of I_0 in the two cases [44,000 versus 400; $\alpha_p^{(1)} \approx 110$], the standard errors of the amplitude and offset parameters also agree well. Thus the experimental results of Table 1 are well mimicked by the simulation parameters.

We conclude from this direct simulation study that the weighted fit is preferred for three reasons: (a) The weighted residuals behave well when the monoexponential model is adequate; in contrast, the observation of systematic deviations of these weighted residuals from randomness or constant variance is an indication of model inadequacy, i.e., nonexponential decay. (b) The weighted fit is more accurate and results in smaller deviations of the estimated parameters. (c) The ratio of the deviation and the standard error is closer to the t_{df} distribution, indicating a larger probability that the estimated parameters are correct.[26]

G. Optimization of the Cavity Alignment

In the subsections above the noise of the decay signal as a consequence of the Poisson-distributed counting process and the related constant α_p were discussed. Inspection of the underlying aspects of α_p reveals unexpected and useful features. The value of α_p, e.g., is a useful parameter for optimizing cavity alignment. Another feature is that α_p can be used to estimate the number of photons in the cavity in the case of a properly aligned cavity.

The initial alignment of the laser beam with respect to the CRD cell and the mirror alignment usually results in a decaying signal. One can often minimize pronounced nonexponential decay and mode beats by monitoring the decay on the oscilloscope while adjusting the cavity alignment. The fine tuning of the alignment, however, is not trivial because nonexponential decay and beat effects are at a certain point no longer discernible by visually monitoring the oscilloscope trace. On-line monitoring of fit parameters and the weighted residuals can help to improve the final fine tuning of the setup. An obvious parameter to monitor during alignment of the CRD cavity appears to be the decay rate, but this can be a pitfall. A low decay rate does not imply good alignment; it can even indicate severe nonexponential decay.

More useful parameters for the fine tuning of the

Table 2. Results (rms average) from Fitting 1024 Simulations of a CRDS Decay[a]

Fit	$\Delta_\beta \times 10^6$	$\hat\sigma_\beta \times 10^6$	Δ_{I_0}	$\hat\sigma_{I_0}$	$\Delta_{I_{off}}$	$\hat\sigma I_{off}$	Root-Mean-Square Error
Unweighted	26	16	2.2	0.9	0.14	0.22	7.3
Weighted	17	17	1.9	1.9	0.08	0.08	1.0

[a]For details see text. The deviations of the estimated parameters, the estimated standard errors, and the rms error of the fit are listed.

cavity alignment are the mean values of the weighted residuals and their standard deviation σ_{res}. In the case of wrongly estimated weight factors, however, these mean values could be satisfactory whereas the weighted residuals are not. It is therefore important to monitor the weighted residuals; only then the mean values and σ_{res} can be interpreted reliably.

Pronounced nonexponential decay and beats or both, with a period comparable with or smaller than one τ ($1/\beta$), will be visible in the residuals of the fit, while fast beatings are often obscured by Poisson noise. A useful measure for the presence of fast beatings is α_p, the parameter already calculated and used in the fitting routine. In ideal circumstances the value for α_p is inversely proportional to the number N of averaged ringdown events per analyzed transient, as follows from Eq. (12):

$$\alpha_p^{(N)} = \frac{\alpha_p^{(1)}}{N}. \tag{16}$$

If stable beatings are present in the decay, they will appear in the residuals when the number of averaged ringdown events increases as the magnitude of the Poisson noise decreases. The beatings will remain in the decay and affect the value of $\alpha_p^{(N)}$ as determined by Eq. (15); the value of $\alpha_p^{(N)}$ will not decrease linearly with N but converges to a constant.

To estimate the expected value of $\alpha_p^{(N)}$ (N is typically 50) of an averaged decay trace, $\alpha_p^{(1)}$ of a single-shot trace has to be determined. From this value the expected value of $\alpha_p^{(N)}$ can easily be determined with Eq. (16). During the fine tuning of the cavity alignment the relevant parameters and the weighted residuals are monitored on-line until they are satisfactory. Alternatively an autocorrelation function or the Fourier-transformed spectrum of the residuals can be used to monitor the residuals. To check the alignment, $\alpha_p^{(1)}$ is again determined. It is possible that due to the fine tuning of the cavity alignment $\alpha_p^{(1)}$ is significantly smaller. The alignment procedure should then be repeated in an iterative way. With this procedure the alignment of the setup can be optimized toward monoexponential decay.

H. Estimation of the Number of Photons Leaking out of the Cavity

A PMT converts the photon flux exiting the cavity into a current. With a rise time of 10 ns and a transit time spread of 22 ns, as in the present experimental setup, the time constants of the PMT are negligibly small compared with the decay time of the photon flux ($\tau = 15$ μs). The PMT signal is sampled by a digitizer without additional amplification or low-pass filtering. Sampling of a signal, however, is not instantaneous; from the specifications of the oscilloscope it is estimated that data points as sampled in the present experiment correspond to an integration of the continuous signal of more than 1–2 ns. Therefore the initial intensity I_0^{fit} estimated from the fit corresponds to the number of photons detected within this bin width, $\Delta t = 1.5 \pm 0.5$ ns. Substitution of $\alpha_p^{(N)}$, determined from the fit, in Eq. (15) gives the gain g of the detection system with which the actual number of photons I_0^{ph} can be calculated:

$$I_0^{ph} = \frac{I_0^{fit}}{\eta \alpha_p^{(N)} N}, \tag{17}$$

where η is the QE of the PMT. The initial flux Φ_0^{ph} that corresponds to a number of photons I_0^{ph} in the first 1.5 ns of the decay is used to calculate the total number of photons by integration of the total decay.

A series of 256 single-shot ($N = 1$) recordings was taken for laser pulses with measured energies of 90 (10) nJ just in front of the entrance mirror; at a wavelength of 630 nm; this corresponds to $2.9\ (0.3) \times 10^{11}$ photons/pulse. Subsequent data analysis gives an average fitted intensity $\bar{I}_0^{fit} = 34.2\ (0.2) \times 10^3$, an average $\bar{\alpha}_p^{(1)} = 123\ (8)$, and an average decay time $\bar{\tau} = 14.52(0.08)$ μs, with the estimated precisions in parentheses. To estimate the number of photons leaking out of the cavity the QE of the PMT and the transmittance of the bandpass filter have to be taken into account, resulting in an average of $2.6(0.9) \times 10^7$ photons exiting the cavity at both sides.

The photon flux can also be estimated from the output current of the PMT. The initial current at the beginning of a decay is on average 418 (6) μA, which corresponds to $2.6(0.4) \times 10^6$ electrons/ns. Taking into account the gain of the PMT, the transit time spread, the QE, and T_{630}, a total number of $2.7(0.5) \times 10^7$ photons in one decay is estimated. The good agreement between the photon numbers derived from the statistical analysis and the PMT output current underlines the correctness of the data-analysis procedure.

4. White Cavity

In many descriptions of the CRD technique in its application to spectroscopy mode structure and optical interference are neglected.[6] The physical picture of the pulses that enter the cavity is then as follows: A laser pulse enters the resonator through the first mirror with an effective transmittance, $T = (1 - R)$, where R is the effective reflectivity estimated from the decay rate. The fraction of the pulse captured in the resonator then gradually leaks out through the mirrors at both ends. In this picture the response of the cavity is white, i.e., the transmission has no frequency dependence. Meijer *et al.*[18] measured the frequency response of a CRD resonator and showed that, in the condition of alignment far from the confocal, the frequency spectrum of the cavity is continuous. Also Scherer *et al.*[30] and Hodges *et al.*[31] have discussed the issue of a white optical resonator.

The data in Section 3 can also be interpreted in terms of the picture of a white cavity. From the estimated decay time, $\tau = 14.52$ μs, a transmittance of $181.0\ (1.4) \times 10^{-6}$ is derived by $T = (1 - R)$. The number of photons coupled into the resonator is then $5.2\ (0.5) \times 10^7$ of which 50% will leak out at the rear side of the cavity: $2.6\ (0.3) \times 10^7$. This result is in good agreement with the previous estimates of the

photon number and thus verifies that the mode structure does not influence the overall transmission property of the cavity; hence the cavity can be considered white.

The data analyzed in Section 3 are taken from measurements at a fixed laser frequency. Data retrieved from a frequency scan (in an empty cavity) with a well-aligned cavity, over several wave numbers and a step size of 0.01 cm^{-1}, are consistent with the data at a fixed laser frequency. This again demonstrates the frequency-independent transmission of the resonator. The data resulting from a scan with a poorly aligned setup vary and are not consistent with the data at a fixed laser frequency.

Characteristic oscillations in the decay rate β as a function of the frequency ν were observed in studies in our laboratory[32] as well as in other reports on CRDS,[20,33] but they never occurred in a CRD spectrum recorded in a setup aligned toward a minimum value of α_p. The oscillations in $\beta_{(\nu)}$ tend to occur in combination with oscillations in I_0 (proportional with the transmitted energy) and may be as high as 40%. Often the oscillations in $\beta_{(\nu)}$ and in I_0 are out of phase. The number of photons estimated by the pulse energy is then inconsistent with the results from estimates based on α_p. In that case the frequency spectrum of the cavity cannot be treated as white because the amount of transmitted energy through the cavity is frequency dependent. If the oscillations are out of phase, they cannot originate from etalon effects in the mirrors, as proposed by Romanini and Lehmann[20]; the phase difference should then be zero. A possible explanation for the out-of-phase behavior of these oscillations could relate to the different losses of different transversal modes[19] in the cavity combined with the transversal mode structure of the laser beam. It is preferred that certain higher-order modes that exhibit higher loss rates might be excited. It is therefore not necessary that the effective reflectivity, the background spectrum, and the intensity are in phase. A final resolution of this issue, often limiting the sensitivity of the CRDS method, has not yet been found.

5. Conclusion and Outlook

In this research it has been demonstrated that the correct analysis of CRD decay transients is far from trivial. The probabilistic properties of the decaying signal and an offset have to be taken into account for a reliable estimation of parameters. Even a small nonzero offset in the decay signal can introduce systematic errors in the estimated decay rate if the offset is not accounted for, e.g., in a linear fit to the logarithm of the decay transient. A simulation study shows that a weighted nonlinear data-analysis procedure, in which all the properties of the decay transients are taken into account, returns the most accurate results with the smallest deviations in the estimated parameters.

A nonlinear fit of the decays to a biased exponential merit function can account for an offset and allows, in principle, for an unlimited fit domain; fixed time settings are superfluous and thus will not influence the results. A mathematical transformation of the data is not necessary; logarithmic transformation of the decay transient can suppress important and interesting features such as noise, oscillations that are due to mode beating, and nonlinearities in the beginning of the decay.

An alignment procedure for the fine tuning of the CRD setup has been developed, based on an on-line evaluation of the fit results and statistical properties of the decay transient. The basic principle of the procedure is alignment toward a setting of monoexponential decay. In certain experimental conditions the frequency spectrum of a CRD cavity is white, a necessary condition for retrieving absolute absorption cross sections with pulsed CRD spectroscopy.[13]

For a well-aligned setup a reliable estimate of the absolute number of photons in the cavity can be given at any time during the decay. With the numbers of photons in the cavity known it is possible to investigate quantitatively intensity-dependent absorptions with the CRD technique. From a first analysis the absolute number of photons can be estimated, preferably with the Poisson constant α_p, and this information can be included in the input of a second, more advanced analysis. Intensity-dependent decay rates have recently been observed in CRD.[34,35]

In this paper laser bandwidth effects have not been discussed. Indeed, for the case in which the bandwidth of the laser source exceeds the widths of molecular resonances the decay transients will exhibit multiexponential decay. This phenomenon has been discussed extensively in the literature.[11–13] Research to extend the present analysis to cover this case is in progress in our laboratory. An important ingredient is the analysis of all decay transients obtained at various frequency settings over the line profile in one procedure; hence an ensemble fit is performed over all data to yield absolute absorption cross sections of narrow molecular absorption features.

Financial support from the Space Research Organization Netherlands (SRON) is gratefully acknowledged.

References

1. A. O'Keefe and D. A. G. Deacon, "Cavity ringdown optical spectrometer for absorption measurements using pulsed laser sources," Rev. Sci. Instrum. **59,** 2544–2551 (1988).
2. A. Kastler, "Atomes à l'intérieur d'un interféromètre Perot–Fabry," Appl. Opt. **1,** 17–24 (1962).
3. T. W. Hänsch, A. L. Schawlow, and P. E. Toshek, "Ultrasensitive response of a cw dye laser to selective extinction," IEEE J. Quantum. Electron. **8,** 802–804 (1972).
4. J. M. Herbelin, J. A. McKay, M. A. Kwok, R. H. Uenten, D. S. Urevig, D. J. Spencer, and D. J. Bernard, "Sensitivity measurement of photon lifetime and true reflectances in an optical cavity by a phase-shift method," Appl. Opt. **19,** 144–147 (1980).
5. J. J. Scherer, J. B. Paul, A. O'Keefe, and R. J. Saykally, "Cavity ringdown laser absorption spectroscopy: history, development, and application to pulsed molecular beams," Chem. Rev. **97,** 25–52 (1997).
6. M. D. Wheeler, S. M. Newman, A. J. Orr-Ewing, and M. N. R.

Ashfold, "Cavity ringdown spectroscopy," J. Chem. Soc. Faraday Trans. **94,** 337–351 (1998).
7. K. K. Lehmann and D. Romanini, "The superposition principle and cavity ringdown spectroscopy," J. Chem. Phys. **105,** 10263–10277 (1996).
8. R. van Zee, J. T. Hodges, and J. P. Looney, "Pulsed, single-mode cavity ringdown spectroscopy," Appl. Opt. **38,** 3951–3960 (1999).
9. J. Martin, B. A. Paldus, P. Zalicki, E. H. Wahl, T. G. Owano, J. S. Harris, C. H. Kruger, and R. N. Zare, "Cavity ringdown spectroscopy with Fourier-transform-limited pulses," Chem. Phys. Lett. **258,** 63–70 (1996).
10. J. Y. Lee, H.-W. Lee, and J. W. Hahn, "Complex traversal time for optical pulse transmission in a Fabry–Perot cavity," Jpn. J. Appl. Phys. **38,** 6287–6297 (1999).
11. R. T. Jongma, M. G. H. Boogaarts, I. Holleman, and G. Meijer, "Trace gas detection with cavity ringdown spectroscopy," Rev. Sci. Instrum. **66,** 2821–2828 (1995).
12. P. Zalicki and R. N. Zare, "Cavity ringdown spectroscopy for quantitative absorption experiments," J. Chem. Phys. **102,** 2708–2717 (1995).
13. J. T. Hodges, J. P. Looney, and R. D. van Zee, "Laser bandwidth effects in quantitative cavity ringdown spectroscopy," Appl. Opt. **35,** 4112–4116 (1996).
14. R. Engeln, G. Berden, R. Peeters, and G. Meijer, "Cavity-enhanced absorption and cavity enhanced magnetic rotation spectroscopy," Rev. Sci. Instrum. **69,** 3763–3769 (1998).
15. B. A. Paldus, C. C. Harb, T. G. Spence, B. Willke, J. Xie, J. S. Harris, and R. N. Zare, "Cavity-locked ringdown spectroscopy," J. Appl. Phys. **83,** 3991–3997 (1998).
16. T. G. Spence, C. C. Harb, B. A. Paldus, R. N. Zare, B. Willke, and R. L. Byer, "A laser-locked cavity-ringdown spectrometer employing an analog detection scheme," Rev. Sci. Instrum. **71,** 347–353 (2000).
17. J. Ye, L.-S. Ma, and J. L. Hall, "Ultrasensitive detections in atomic and molecular physics; demonstration in molecular overtone spectroscopy," J. Opt. Soc. Am. B **15,** 6–15 (1998).
18. G. Meijer, M. G. H. Boogaarts, R. T. Jongma, D. H. Parker, and A. M. Wodtke, "Coherent cavity ringdown spectroscopy," Chem. Phys. Lett. **217,** 112–116 (1994).
19. J. L. Remo, "Reflection losses for symmetrically perturbed curved reflectors in open resonators," Appl. Opt. **20,** 2997–3002 (1981).
20. D. Romanini and K. K. Lehmann, "Ringdown-cavity absorption spectroscopy of the very weak HCN overtone bands with 6, 7, and 8 stretching quanta," J. Chem. Phys. **99,** 6287–6301 (1993).
21. A. O'Keefe, "CW integrated cavity output spectroscopy," Chem. Phys. Lett. **293,** 331–336 (1998).
22. A. O'Keefe, J. J. Scherer, and J. B. Paul, "Integrated cavity output analysis of ultraweak absorption," Chem. Phys. Lett. **307,** 343–349 (1999).
23. *Photomultiplier Tubes*, (Catalog) (Hamamatsu Photonics, Shizuoka Prefecture, Japan, 1996).
24. W. H. Press, S. A. Teukolsky, W. T. Vetterling, and B. P. Flannery, *Numerical Recipes in C: The Art of Scientific Computing*, 2nd ed. (Cambridge University, Cambridge, England, 1993).
25. Y. Beers, *Introduction to the Theory of Error* (Addision-Wesley, Cambridge, Mass., 1957).
26. D. M. Bates and D. G. Watts, *Nonlinear Regression and its Applications* (Wiley, New York, 1988).
27. R. J. Carroll and D. Ruppert, *Transformation and Weighting in Regression* (Chapman & Hall, New York, 1988).
28. I. H. M. van Stokkum, W. A. van der Graaf, and D. Lenstra, "Weighted fit of optical spectra," Opt. Commun. **121,** 103–108 (1995).
29. *Splus Reference Manual* (Statistical Sciences, Seattle, Wash., 1991).
30. J. J. Scherer, D. Voelkel, D. J. Rakestraw, J. B. Paul, C. P. Collier, R. J. Saykally, and A. O'Keefe, "Infrared cavity-ringdown spectroscopy laser-absorption spectroscopy (IR-CLAS)," Chem. Phys. Lett. **245,** 273–280 (1995).
31. J. T. Hodges, J. P. Looney, and R. D. van Zee, "Response of a ringdown cavity to arbitrary excitation," J. Chem. Phys. **105,** 10278–10288 (1996).
32. H. Naus, A. de Lange, and W. Ubachs, "$b^1\Sigma_g^+ - X^3\Sigma_g^-$ (0,0) band of oxygen isotopomers in relation to tests of the symmetrization postulate in $^{16}O_2$," Phys. Rev. A **56,** 4755–4763 (1997).
33. M. G. H. Boogaarts and G. Meijer, "Measurement of the beam intensity in a laser-desorption jet-cooling mass-spectrometer," J. Chem. Phys. **103,** 5269–5274 (1995).
34. I. Labazan, S. Rustić, and S. Milošević, "Nonlinear effects in pulsed cavity-ringdown spectroscopy of lithium vapor," Chem. Phys. Lett. **320,** 613–622 (2000).
35. C. R. Bucher, K. K. Lehmann, D. F. Plusquellic, and G. T. Fraser, "Doppler-free nonlinear absorption in ethylene by use of continuous-wave ringdown spectroscopy," Appl. Opt. **39,** 3154–3164 (2000).